The nature of the highest energy cosmic rays

Todor Stanev[1] & H.P. Vankov

[1] *Bartol Research Institute, University of Delaware, Newark, DE 19716*

[2] *Institute for Nuclear Research and Nuclear Energy, Sofia ##, Bulgaria*

Ultra high energy gamma rays produce electron–positron pairs in interactions on the geomagnetic field. The pair electrons suffer magnetic bremsstrahlung and the energy of the primary gamma ray is shared by a bunch of lower energy secondaries. These processes reflect the structure of the geomagnetic field and cause experimentally observable effects. The study of these effects with future giant air shower arrays can identify the nature of the highest energy cosmic rays as either γ–rays or nuclei.

PACS numbers: 98.70.Sa, 96.40.De, 91.25, 96.40.Pq

I. INTRODUCTION

Ever since the reports of the detection of two cosmic ray showers of energy well above 10^{20} eV [1,2] the origin and the nature of such events have been subjects of strong interest and intense discussion. It is not only very difficult [3] to extend our understanding of particle acceleration to such extraordinarily high energies but the propagation of these particles in the microwave background and possibly other universal radiation fields restricts the distance to their potential sources to several tens of Mpc.

Conservatively minded astrophysicists are looking for astrophysical sources which may contain the environment necessary for stochastic particle acceleration to energies in excess of 10^{20} eV. Powerful (FRII) radio galaxies [4] have been suggested as possible sources. If this suggestion were true, the highest energy cosmic rays (HECR) would be most likely protons, reflecting the composition of the matter that is available for injection in the termination shocks of FRII jets. Others [5] search for powerful astrophysical sources in the cosmologically nearby Universe. HECR then could also be heavier nuclei, for which the acceleration is less demanding. The propagation of heavy nuclei on short distances (O(10) Mpc) without huge energy loss is possible.

Some cosmologists relate the origin of HECR to topological defects [6]. Topological defects (TD) scenarios avoid the problems of particle acceleration since they are based on 'top–down' evolution. Very massive ($10^{22} - 10^{25}$ eV) X–particles are emitted by the topological defects that later decay into baryons and mesons of lower energy. Most of the energy is eventually carried by γ–rays and neutrinos, that are products of meson decay. Detected HECR would then most likely be γ–rays.

Most radically, the origin of HECR has been related to those of gamma ray bursts [7–9], replacing two extremely luminous mysteries with a single one. In such scenarios HECR are most likely to be again protons. We may not be able to observe the sources of HECR since every source might only emit a single observed ultrahigh energy particle.

The nature, the type of the particle that interacted in the atmosphere to generate these

giant air showers, could be the key to the understanding the origin of the highest energy cosmic rays. The current experimental evidence on the nature of HECR is not conclusive. The Fly's Eye experiment, for example, has reported correlated changes in the spectra and the composition of the ultra high energy cosmic rays [10]. The analysis of the Fly's Eye experimental statistics suggests that a change of the chemical composition of the cosmic rays from heavy nuclei to protons at $\sim 3 \times 10^{18}$ eV is accompanied by a change of the spectral index of the cosmic ray energy spectrum. One may then conclude that the HECR are protons. The other currently running air shower experiment, AGASA, does not observe [11] such a correlation. A re–analysis of the archival data from the SUGAR experiment [12] makes the opposite conclusion – a large fraction of the highest energy showers seem to be generated by heavy nuclei..

A correlation between the arrival directions of HECR with energy $> 4 \times 10^{19}$ eV with the supergalactic plane, that contains most of the galaxies of redshift < 0.03, has been reported [13]. The AGASA experiment has also observed similar correlation in their data set [14], although not fully consistent with the conclusions of Ref. [13]. On the other hand the Fly's Eye experiment does not see such a correlation (P. Sommers for the Fly's Eye group, *private communication*). It also has not been observed in the SUGAR data [15]. Even if confirmed in the future, a correlation with the structure of the local universe would not answer the question of the nature of HECR. If topological defects are seeds for galaxy formation most powerful galaxies and TD would have similar distribution and TD and astrophysical scenarios of the origin of HECR are indistinguishable.

The profile of the $3{\times}10^{20}$ eV shower detected by the Fly's Eye develops higher in the atmosphere than expected for either proton or γ–ray showers of that energy [16]. The highest energy shower seen by the AGASA experiment (2×10^{20} eV) exhibits, apart from its energy, features that are typical for most of the high energy showers. The currently existing air shower arrays cannot drastically increase the experimental statistics and the hope for answering the important questions for the nature and origin of HECR is in the construction of much bigger shower arrays, such as the Auger project [17].

Even with Auger, however, the nature of HECR will be difficult to study. Shower parameters are subject of strong intrinsic fluctuations and the cross sections that govern inelastic interactions at $\sqrt{s} = 100$ TeV are not well enough known. At lower energy ($10^{14} - 10^{16}$ eV) showers generated by heavy nuclei, protons and γ–rays could be at least statistically distinguished by their muon content. γ–ray showers have on the average $\sim 3\%$ of the muon content of proton showers of the same energy [18]. At ultrahigh energies such approach may not be possible – calculations of the muon content of the γ–ray induced showers predict that the fraction of GeV muons could be even higher than in proton generated showers [19,20].

We suggest a different approach to the study of the nature of the cosmic rays with energy above 10^{19} eV – to prove (or disprove) that HECR are γ–rays by observing their interactions with the geomagnetic field. While protons and heavier nuclei are not affected by the geomagnetic field, ultra high energy γ–rays interact on it to produce e^+e^- pairs. The electrons themselves quickly lose their energy through magnetic bremsstrahlung (synchrotron radiation) before they enter the atmosphere of the earth. Air showers are thus replaced by 'magnetic + atmospheric' showers that start far away from the surface of the earth and are absorbed faster compared to usual air showers. With high experimental statistics one can observe the interactions of ultra high energy γ–rays with the geomagnetic field by a study of the shower arrival direction in geographical coordinates. If the detected showers do not show signs of interactions with the geomagnetic field, the suggestions for γ–ray nature of HECR could be proven wrong.

This article is organized in the following way. Section 2. gives a brief discussion of the photon and electron interactions on magnetic fields and of the structure of the geomagnetic field. Section 3. describes a calculation of the 'geomagnetic + atmospheric' cascades and gives some general results of that calculation. Section 4. calculates shower parameters that could be used to confirm the γ–ray origin of HECR and Section 5. contains the conclusions from this research.

II. PHOTON AND ELECTRON INTERACTIONS IN THE GEOMAGNETIC FIELD

Interactions of photons, and especially of electrons, on magnetic fields have been exhaustively studied because of all the problems they create in particle accelerators. The theoretical and some experimental knowledge is reviewed by T. Erber in Ref. [21].

Magnetic pair production is guided by the parameter $\Upsilon_\gamma \equiv [1/2][h\nu/mc^2][B_\perp/B_{cr}]$, where $B_{cr} \equiv m^2c^3/e\hbar = 4.414 \times 10^{13}$ Gauss and $B_\perp$ is the component of the magnetic field that is normal to the γ–ray trajectory. The γ–ray attenuation coefficient, i.e. the fraction of photons that undergo pair production in magnetic field of strength $B_\perp$ per unit distance is given by

$$\alpha_\gamma(\Upsilon_\gamma) \;=\; 0.16\frac{\alpha mc}{\hbar}\frac{mc^2}{h\nu}K^2_{1/3}(2\Upsilon_\gamma/3)\mathrm{cm}^{-1} \tag{1}$$

The maximum attenuation is reached at γ–ray energy of $12mc^2(B_{cr}/B_\perp)$ while the cross section of the process is linearly proportional to the magnetic field strength $B_\perp$.

Similarly the magnetic bremsstrahlung (synchrotron radiation) is guided by $\Upsilon_e \equiv [E/mc^2][B_\perp/B_{cr}]$. The radiation emitted by an electron of energy E_e in magnetic field $B_\perp$ per unit distance is distributed as

$$I(E_e, h\nu, B_\perp) \;=\; \frac{sqrt3\alpha}{2\pi}\frac{m^2c^3}{\hbar}\frac{\Upsilon_e}{E}\left(1-\frac{h\nu}{E_e}\right)K(2J)\;, \tag{2}$$

where $J \equiv [h\nu/E_e][1 + h\nu/E_e]/3\Upsilon_e$.

To demonstrate the strength of the γ–ray interactions in the geomagnetic field we show in Fig. 1 the distributions of the distances from the surface of the earth at which γ–rays of different energy pair produce. The γ–ray trajectory is taken to be normal to the field lines of a magnetic dipole centered at the center of the Earth with magnetic moment of 8.1×10^{19} Gauss/m. One could see that the γ–rays of the energies of interest interact in a relatively narrow range of distances not further than $3R_\oplus$. The narrow peak plotted at altitude of 20 km represents γ–rays that survive, i.e. interact in the atmosphere before they interact in

the geomagnetic field. 12% of the γ–rays with energy 10^{20} eV (and none at higher energy) survive.

The spectra of the γ–rays emitted in magnetic bremsstrahlung depends quite strongly on the magnetic field strength. For strong fields the energy distribution of the secondary photons is quite flat. Fig. 2 shows the energy loss of 10^{20} electrons in magnetic fields of strength $\log_{10} B_\perp = -0.5, -1, -1.5$, etc. Gauss as a function of the secondary photon energy. In the dipole field model described above a field of 0.1 Gauss corresponds to a distance of 0.468 $R_\oplus$ above the surface of the earth, and 0.032 Gauss – to 1.15 $R_\oplus$. These distances cover much of the primary γ–rays interaction range shown in Fig. 1. Since lower energy γ–rays pair produce close to the earth, the magnetic bremsstrahlung of their secondary electrons is harder. The energy spectra of the γ–rays in the bunch that enters the atmosphere after pair production and magnetic bremsstrahlung tend to be almost independent of the primary γ–ray energy E_γ^0.

A. Structure of the geomagnetic field

Gamma rays arriving at any experimental location under different zenith (ϑ) and azimuthal (ϕ) angle will see a different geomagnetic field. They will thus cascade differently before reaching the atmosphere. At small ϑ, close to the vertical direction, the variation with ϕ is insignificant. At relatively large ϑ, more than 30°, the field strength for most locations changes by factors of 3 or more for different values of ϕ.

A more quantitative calculation of the strength of the field encountered by the incoming γ–ray is trivial for any model of the geomagnetic field but has to be performed for each location, ϑ and ϕ separately. We have attempted to obtain a slightly more general result for several experimental locations. Fig. 3 shows the transverse component ($B_\perp$) of the geomagnetic field as a function of the azimuthal angle at which it arrives to the detector. Since the ϕ variations for different zenith angles ϑ have the same aspect, we have integrated over ϑ from 0 to 60°, weighting the field values with the solid angle. The 1991 International

Geomagnetic Reference Field model (IGRF) is used for this calculation.

Four of the locations for which $B_\perp$ is shown are in the Northern hemisphere and only one (Sydney, shown with dash–dash) is South of the equator. Since the smallest $B_\perp$ is seen in the direction of the magnetic pole that is closer to each location, northern and southern locations have opposite field strength dependence on ϕ. At the moderate latitudes of these detector locations, the detailed differences between the Northern hemisphere detectors are minor. (A detector located at the geomagnetic equator would have a symmetric response to geomagnetic North and South directions). The difference between the maximum and minimum field strengths is almost a factor of 5.

For each one of these detectors, as well as for any other detector location, one could determine a region in azimuth, where the field strength is the lowest and the incoming γ–rays would be affected minimally by the geomagnetic field and a region where the effect of the geomagnetic field is at maximum. For the location of Sydney, e.g. γ–rays arriving with $130^\circ < \phi < 215^\circ$ would see $B_\perp$ <0.02 Gauss at a distance of 1 $R_\oplus$ and γ–rays with $255^\circ < \phi < 90^\circ$ would see more than 0.04 Gauss at the same distance. The idea is that γ–ray fluxes arriving from these two regions may have observable characteristics that are different enough to be distinguished experimentally. We continue to study the cascading of ultra high energy gamma rays in geomagnetic fields with different strength, corresponding to these two regions.

III. CASCADING IN THE GEOMAGNETIC FIELD

We simulate the electromagnetic cascading in the geomagnetic field by injecting γ–rays of energy E_γ^0 at a distance of 5 $R_\oplus$ from the surface of the earth on a trajectory with angle ϑ relative to the vertical direction at the intersection with the surface. The γ–ray is propagated with a stepsize Δx (from 1 to 10 km) until the γ–ray pair produces or reaches the atmosphere. The atmosphere is defined to be at altitude of 20 km above the earth's surface. Gamma rays that reach the atmosphere 'survive' and interact in the atmosphere to

produce air showers with their original injection energy.

If the γ–ray produces an electron–positron pair, the pair electrons are followed in similar way, by calculating their radiation spectrum on every step of propagation. The synchrotron γ–rays are tabulated in energy, starting at 10^{14} eV. The assumption here is that secondary γ–rays of energy less than 10^{14} eV do not contribute significantly to the cascades that are observed deep in the atmosphere. This lower energy end of the magnetic bremsstrahlung spectrum, as well as the electrons of energy below 10^{14} eV that enter the atmosphere, contain always less than 2% of the primary γ–ray.

Each particle produced in the geomagnetic field, as well as the 'surviving' primary γ–rays then generate atmospheric cascades. The profiles of these cascades are added up to calculate the composite shower profile, generated in the atmosphere by the injected primary γ–ray or the products of its interaction in the geomagnetic field.

The actual calculation is performed using the dipole magnetic field model with magnetic moment of 8.1×10^{19} Gauss/m with two scale factors of 0.25 (low field) and 1.25 (high field), which generate magnetic field strengths approximately equal to the maximum and minimum values shown in Fig. 3.

To study the 'survival' probability in these two field models we made calculations for two extreme zenith angles: $\vartheta = 0^\circ$ and 60°, which is the maximum zenith angle at which air showers can be reliably detected and analyzed. Fig. 4 shows the survival probabilities at high (lefthand strip) and low magnetic field strengths. The lefthand boundary of each strip corresponds to propagation at $\vartheta = 60^\circ$ and the righthand boundary is for $\vartheta = 0^\circ$. γ–rays approaching the earth at higher zenith angles spend significantly more time in higher geomagnetic field strengths and have a higher interaction probability. The lefthand edge of the high field strip and the righthand edge of the low field strip practically bracket the survival probability space for γ–rays approaching any location at the earth surface with zenith angles smaller than 60°. γ–rays arriving at higher angles may be absorbed faster.

Several calculations of the γ–ray cascading in the geomagnetic field have been previously performed [22,20,23]. Our results are in a good agreement with the main results of all

of them. Our calculation is generally a refinement of previous ones, which nevertheless reveals some practically important features in the cascading process. Previous calculations conclude that there will be a 'cutoff' in the energy spectrum of the γ–rays that reach the atmosphere, because of the very soft spectrum of the secondary photons, generated by magnetic bremsstrahlung. This conclusion is partially due to the relatively rough treatment and low statistics in the previous work. Fig. 5 shows the number of secondary γ–rays and the energy that they carry. $E_\gamma^0 = 3\times10^{20}$ eV in this example. Although the number of secondary γ–rays of energy above 10^{19} eV is on the average only 6.3, they carry 48% of the primary energy. This is also important for the development of the subsequent air showers, because at energies above 10^{19} eV the LPM effect [24], which suppresses the electromagnetic cross sections at high energy and slows the development of the air showers, becomes important in air.

IV. ATMOSPHERIC SHOWERS

Gamma rays of energy above 10^{19} eV, if they do exist, would only be detectable by giant air shower arrays located on the surface of the earth. Air shower arrays consist of a large number of counters that trigger in coincidence when the shower from arrives. The shower direction is determined by the arrival time of the shower front at the different counters. A fit of the density in the separate counters reconstructs the total number of shower particles, the showers size N_e, which is then used to determine the primary energy.

The output of our Monte Carlo simulation includes the shower sizes calculated for several atmospheric depths from the cascading of all secondary (and primary, if the injected gamma rays did not pair produce) γ–rays in the atmosphere. The profiles from individual secondary γ–rays of energy above 10^{18} eV are calculated with an account for the LPM effect, although the effect is not significant below 10^{19} eV. The depths are arbitrarily chosen to include a realistic range for typical large air shower experiment and correspond to an array at vertical depth of 860 g/cm^2 and zenith angles with $\cos\vartheta = 0.9$, 0.8, 0.7, 0.6 and 0.5. Because the

development of purely electromagnetic showers in the atmosphere (apart from their muon content) does not depend significantly on the atmospheric density profile, the examples given below could be scaled also to different altitudes and zenith angles.

Fig. 6 shows a general and important shower parameter – the average size ($< N_e >$) generated by γ–rays of different energy. The solid lines are for low field (scale factor of 0.25) and the dashed lines are for high field (scale factor of 1.25). From top to bottom the lines show $N_e(E_\gamma^0)$ at the 5 different depths of 956, 1075, 1229, 1433 and 1720 g/cm^2. Except for the deepest observation level, N_e is multiplied by the factor shown by each curve to make the figure readable. In the absence of interactions in the geomagnetic field, and for lower E_γ^0, the shower size have a power low dependence on E_γ, $N_e = E_\gamma^\alpha$ with $\alpha >1$. The power law index α depends on the column density between the depth of the shower maximum X_{max} and the detector. The size at maximum N_{max} is exactly proportional to E_γ^0 and α is bigger than unity because the depth of shower maximum grows with energy as $X_{max} = \log(E_\gamma^0/81\mathrm{MeV})$ radiation lengths (1 r.l. = 37.1 g/cm^2 in air).

The dependence shown in Fig. 6 is more complicated because in this energy range showers are already at or before their maximum development at some of the shallower observation levels. The role of the magnetic field strength on the N_e dependence on E_γ^0 is easier to understand for the deepest levels of observation. Compare, for example, the two curves for depth of 1720 g/cm^2 with the γ–ray survival probability of Fig. 4. At low energy, where there are no interactions on the geomagnetic field, the two curves are the same. The solid curve (low field) starts bending at γ–ray energy 2×10^{20} eV where the primary γ–rays start interacting in the geomagnetic field. Because of these interactions the primary γ–ray is replaced by a bunch of γ–rays of lower energy. The composite shower reaches maximum at shallower atmospheric depths and is significantly absorbed at the deep observation level. The same happens at energy lower by about one order of magnitude in the high field case. Although it is outside of the energy range of Fig. 6, at some higher energy, where all γ–rays interact on the geomagnetic field, the two curves will join again.

To explain the behaviour at the shallow observation levels one has to take into account

some of the details of the cascading in the geomagnetic field, namely the shape of the energy spectra of the secondary photons as a function of field strength, which is shown in Fig. 2. Although the primary γ–rays interact in the same way, in the high field case the energy spectra of the secondary γ–rays are harder, hard enough to generate showers that are not absorbed at the level of 956 g/cm^2. One could hardly see a tiny deviation of the strong field (dashed) curve in the region of $E_\gamma^0 = 3 \times 10^{19}$ eV. At higher energies the secondaries are energetic enough to produce N_e dependence very close to a power law. When the primary γ–rays start interacting in the low field, however, the picture is slightly different. The secondary γ–ray spectra are softer, the composite showers reach maxima at shallower depths and are correspondingly absorbed when they reach the observation level. The two curves will join asymptotically.

All other levels show intermediate behaviour where the relation between the depth of observation and X_{max} also contributes to the exact shape of the curve.

Fig. 6 shows the strong differences in the observable parameter N_e which is introduced by the strength of the geomagnetic field. It can not be used, however, for analysis of experimental data because E_γ^0 is not a directly measurable parameter. What experiments can do, and usually do, is to produce a spectrum of the measured shower sizes N_e. Such spectra for the three deeper observation levels are shown in Fig. 7. The solid histogram corresponds to the low field and the dashed one – to the high field case.

The histograms are result of a simulation, where E_γ^0 is sampled from a $(E_\gamma^0)^{-2}$ differential primary spectrum between 10^{19} and 10^{21} eV. At low N_e the spectra are always higher for the low field case, including the two observation levels that are not shown in Fig. 7. At the high N_e side and for shallow observation levels the high field case shows higher spectrum, as could be expected by the results shown in Fig. 6 and as seen for the shallowest level plotted in Fig. 7. The biggest difference is at the deepest observation level, where the spectra are different as much as a factor of 10. The differences between the size spectra decreases for shallower observation levels, and is probably not detectable for the two shallowest levels, which are not shown.

V. DISCUSSION AND CONCLUSIONS

The size spectra of Fig. 7 show that it is possible to detect the difference between a flux of γ–rays that reach the earth after cascading in geomagnetic field of different effective strength. In practical terms this means that any experiment that is able to collect large enough experimental statistics should see different N_e spectra in different azimuthal directions if HECR are indeed γ–rays. We have not attempted to look for this effect in the existing experimental statistics, because it is not large enough to reveal such effects.

The Auger project [17] is an entirely different story. It proposes the construction of two air shower arrays, at least 3 000 km^2 each, in the Northern and in the Southern hemisphere. For comparison, the area of the largest current detector (AGASA) is 100 km^2. Each one of these detectors will have the collecting power of more than 5 000 showers above 10^{19} eV per year. If the HECR primaries are γ–rays the Norther hemisphere detector should see spectra similar to the low field case of Fig. 7 in northern direction (the exact direction and value of the minimum field depends on the location of the array) and the strong field case in showers coming from South. The southern detector will have the opposite effect. If this were the case, the difference of the size spectra would prove that the HECR are gamma rays.

The actual effects could even be stronger than shown in Fig. 7, because the simulation on which it is based propagated all primary γ–rays along the vertical ($\vartheta = 0°$) direction. In fact, as shown in Fig. 4, the increase of the interaction probability in the geomagnetic field increases by a non–negligible factor when the exact particle trajectory is accounted for. Our air shower simulation also does not account for the magnetic bremsstrahlung of the shower electrons which at high E_e and low atmospheric density $< 10^{-5}$ g/cm^3 could be important and could accelerate the shower development.

In principle the interplanetary magnetic field has to be added to the 'target' magnetic field. Gamma ray arriving from a cone centered on the Sun would be absorbed far away from the earth and possibly not detectable. The sun could thus be visibly in ultra high energy γ-rays. The exact dimensions of the region where γ–rays are absorbed in pair production on

the solar magnetic field, carries valuable information on the magnetic field in the vicinity of the sun. This is an interesting although purely academic problem, because the statistics of such events is always going to be negligible.

Although we have not done it for this paper, there will be effects, similar to the N_e ones, on the muon content of the γ–ray initiated air showers. It is well known that at these extremely high energies the number of soft muons (0.3 to 2 GeV) in γ initiated showers is comparable to this of hadronic showers [19,20]. The number of soft muons has an E_γ^0 dependence very similar to N_e, because the low energy muons decay readily when X_{max} is distant from the observation level. The decay length of 1 GeV muons is $\sim$6 km. A picture similar to the N_e spectra in Fig. 7 will develop as a result of the cascading in geomagnetic fields of different effective strength. The major difference between the behaviour of the electron size and the muon size is that N_e attenuates as a function of the column density, while N_μ attenuates as a function of the distance, i.e. N_μ will depend strongly on the shower zenith angle ϑ.

The study of the two major components of the giant air showers can reveal the nature of the highest energy cosmic rays. If the specific dependence on the shower arrival direction is observed, then the highest energy cosmic rays are γ–rays. A non observation of this effect would leave us with the choice between protons and heavy nuclei.

Acknowledgements. TS is grateful to A.A. Watson for inspiring discussions on the subject of giant air shower. The work of TS is supported in part by the U.S. Department of Energy under contract DE-FG02-91ER40626. HPV is thankful to US NSF for partial support of his visit to U.S. where this work was conceived, and to the Bartol Research Institute for its hospitality.

REFERENCES

[1] D.J. Bird *et al., Phys. Rev. Lett.* **71**, 3401 (1993).

[2] N. Hayashida *et al., Phys. Rev. Lett.* **73**, 3491 (1994).

[3] A.M. Hillas, *Ann. Revs. Astr. Astrophys.*, **22**, 425 (1984).

[4] J.P. Rachen and P.L. Biermann, *Astron. Astrophys.* **272**, 161 (1993); J.P. Rachen, T. Stanev and P.L. Biermann, *Astron. Astroph.* **273**, 377 (1993).

[5] S.S. Al–Dargazelli *et al. J. Phys. G: Nucl. Part. Phys*, submitted; J. Szabelski, J. Wdowczyk & A.W. Wolfendale, *J. Phys.G: Nucl.Phys.* **12**, 1443 (1986).

[6] P. Bhattacharjee, C.T. Hill and D.N. Schramm, *Phys. Rev. Lett.*, **69**, 567 (1992); G. Sigl, D.N. Schramm and P. Bhattacharjee, *Astropart. Phys.* **2**, 401 (1994).

[7] E. Waxman, *Phys. Rev. Letters*, **75**, 386 (1995).

[8] M. Vietri, *Ap. J.* **453**, 883 (1995).

[9] M. Milgrom and V. Usov, *Ap. J.* **449**, L37 (1995).

[10] D.J. Bird *et al.* Phys. Rev. Lett. 71, 3401 (1993).

[11] N. Hayashida *et al. J. Phys. G: Nucl. Part. Phys.*, **21** 1101 (1995).

[12] X. Chi, J. Wdowczyk & A.W. Wolfendale, *J. Phys. G: Nucl. Part. Phys.* **18** (1992) and references therein.

[13] T. Stanev *et al., Phys. Rev. Lett.*, **75**, 3056 (1995).

[14] N. Hayashida *et al.* (The AGASA collaboration) *Phys. Rev. Lett*, submitted.

[15] L.J. Kewley, R.W. Clay & B.R. Dawson, *Astropart. Phys.*, in print.

[16] F. Halzen *et al., Astropart. Phys.* **3**, 151 (1995).

[17] See "Cosmic Rays Above 10^{19} eV – 1992", eds. M. Boratav *et al. Nucl. Phys.* **28B**

(1992); "The Pierre Auger Project", Design Report, The Auger Collaboration (1995).

[18] T.K. Gaisser *et al., Phys. Rev.*, **D43**, 314 (1991).

[19] T.J.L. McComb, R.J. Protheroe & K.E. Turver, *J. Phys. G: Nucl. Phys*, **5**, 1613 (979).

[20] F.A. Aharonian, B.L. Kanewski & V.V. Vardanian, *Astrophys. Sp. Sci.*, **167**, 111 (1990).

[21] T. Erber, *Revs. Mod. Phys.*, **38**, 626 (1966).

[22] B. McBreen & C.J. Lambert, *Proc. 17th Int. Cosmic Ray Conf.* (Paris) **6**, 70 (1981).

[23] H.P. Vankov and P.V. Stavrev, *Phys. Lett. B*, **266**, 178 (1991).

[24] See T. Stanev *et al., Phys. Rev.* **D25**, 1291 (1982) for the influence of the LPM effect on the shower development.

FIGURES

FIG. 1. Distribution of the interaction points of γ–rays of energy 10^{21} eV (solid line), 3.16×10^{20} eV (dotted line) and 10^{20} eV (dashed line). The interaction points are the vertical distances from the surface of the earth. The shading in the left hand side of the figure represents the atmosphere.

FIG. 2. Energy loss of 10^{20} eV electrons as a function of the strength of the magnetic field and the energy of the secondary photons. The field strength is indicated by the respective curve as $\log_{10}(B_\perp/\text{Gauss})$.

FIG. 3. The strength of the geomagnetic field component that is perpendicular to the γ–ray trajectory as a function of the azimuthal angle ϕ at which the particle arrives at the location is shown for a distance of 1 $R_\oplus$ from the detector. The field strength is integrated over zenith angles ϑ from 0 to 60° accounting for the solid angle. The calculation is performed for the locations of several air shower arrays: a.) Fly's Eye (40N, 112W) – solid line; b.) Yakutsk (62N, 129E) – dots; c.) Akeno (35N, 138E) – dashes; d.) Haverah Park (54N,2W) – dash–dot; e.) Sydney (30S, 150E) – dash–dash. The 1991 IGRF model of the geomagnetic field is used in this calculation.

FIG. 4. Survival probability for γ–rays of energy between 10^{19} and 10^{21} eV in the dipole geomagnetic field model described in the text with scaling factors of 0.25 (righthand strip) and 1.25 (lefthand strip). The lefthand edge of each strip shows the survival probability for γ–rays approaching the surface of the earth with a zenith angle $\vartheta = 60°$ and the righthand edges are for $\vartheta = 0°$.

FIG. 5. Energy spectrum of the secondary γ–rays that reach the atmosphere after the cascading of a primary γ–ray of energy 3×10^{20} eV – solid line, lefthand scale. The dotted histogram and the righthand scale show the amount of energy carried by the secondary γ–rays in each bin.

FIG. 6. Relation between the average shower size N_e and the primary γ–ray energy E_γ^0 for the five observation levels defined in the text for cascading in high (solid) and low (dashed line) strengths of the geomagnetic field. N_e values are multiplied by the factor indicated by the curves.

FIG. 7. Integral shower size N_e spectra generated by primary γ–rays sampled on a $(E_\gamma^0)^{-2}$ differential spectrum between 10^{19} and 10^{21} eV. The solid histograms show the low field case and the dashed histograms are for high field. The observation levels are 1720, 1433, and 1229 g/cm^2 from left to right.

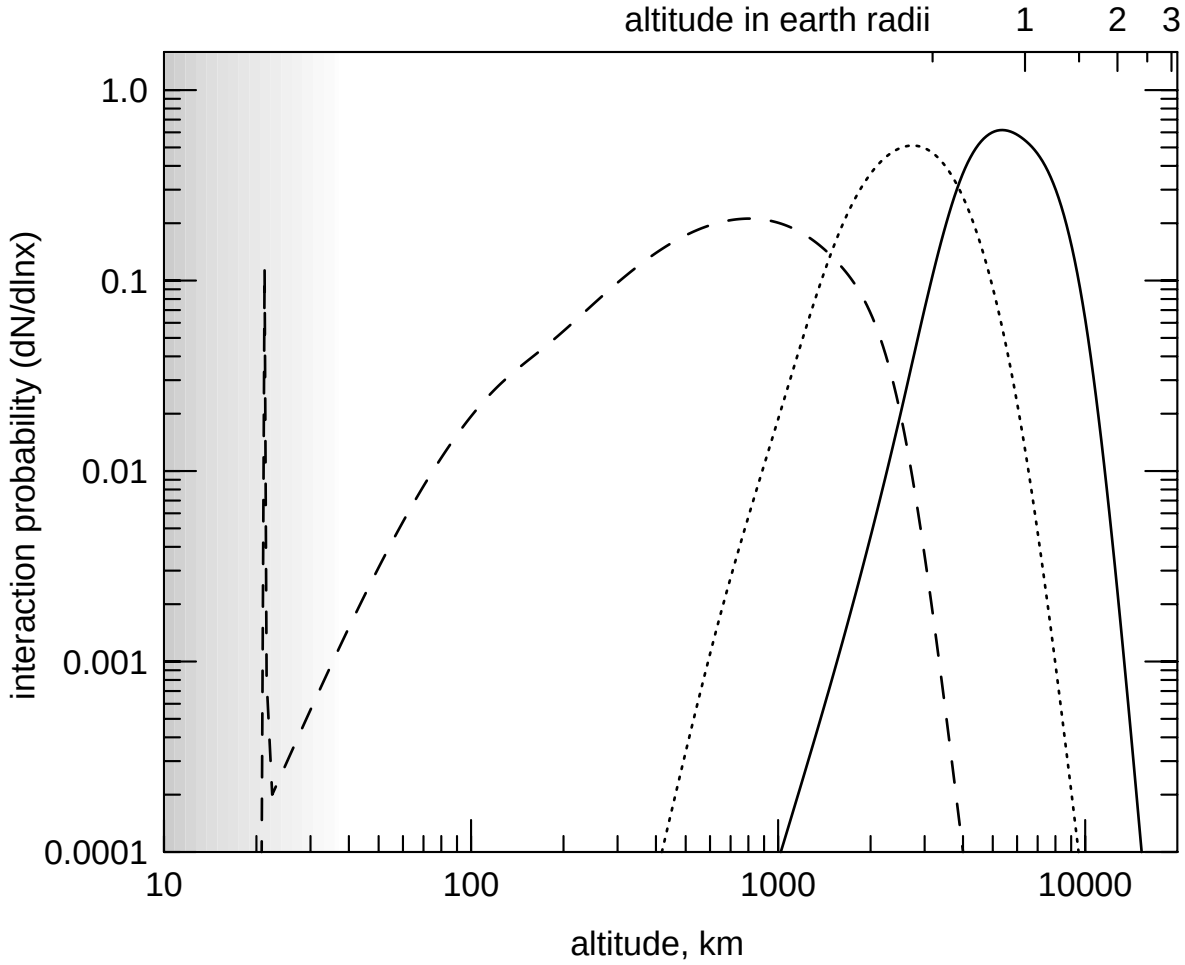

Stanev & Vankov, Fig. 1

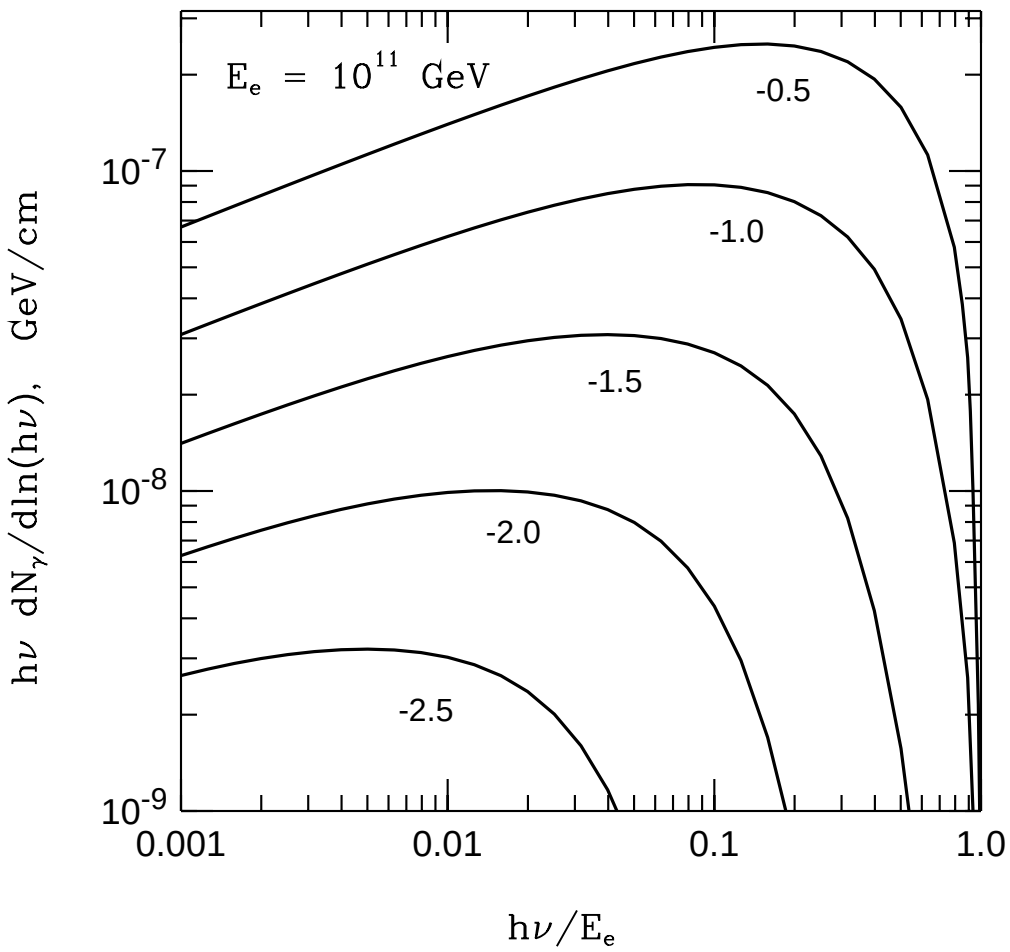

Stanev & Vankov, Fig. 2

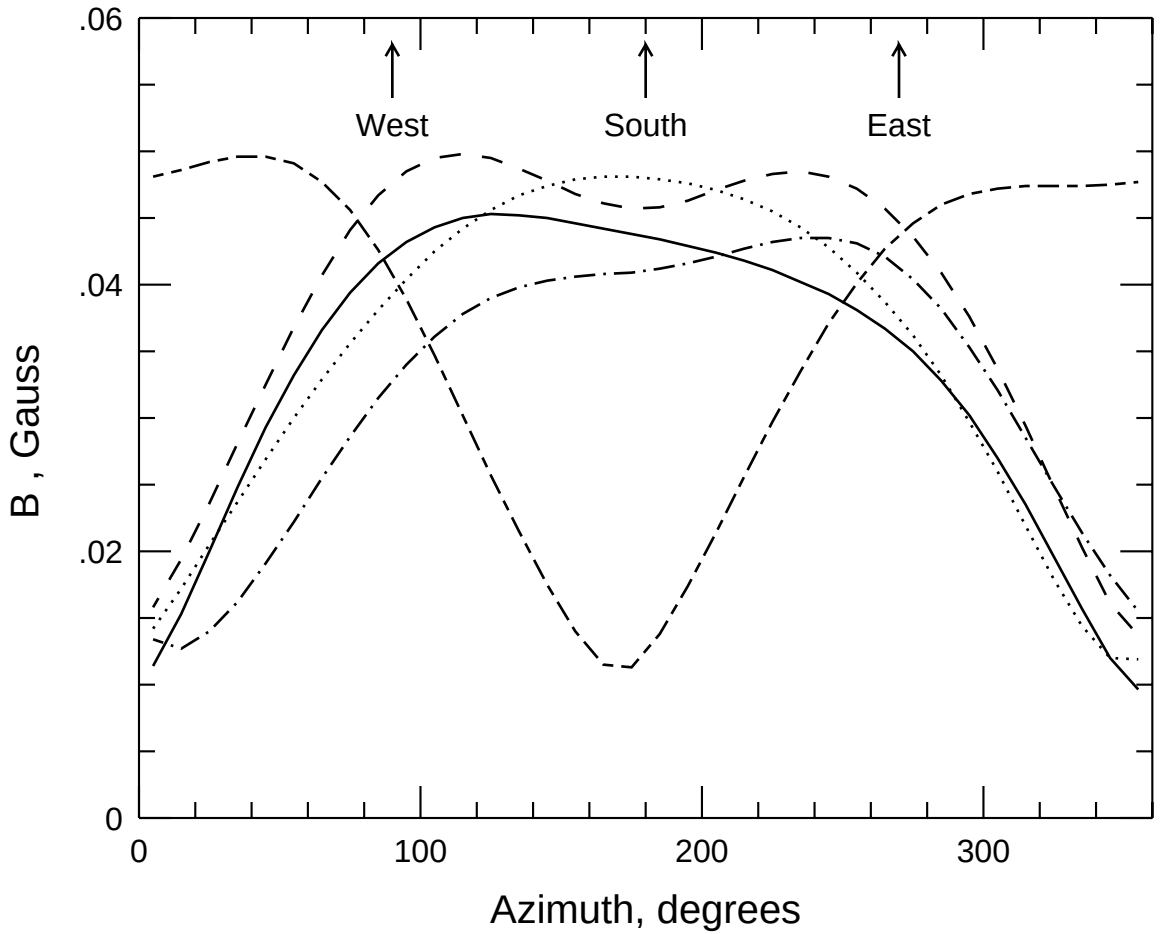

Stanev & Vankov, Fig. 3

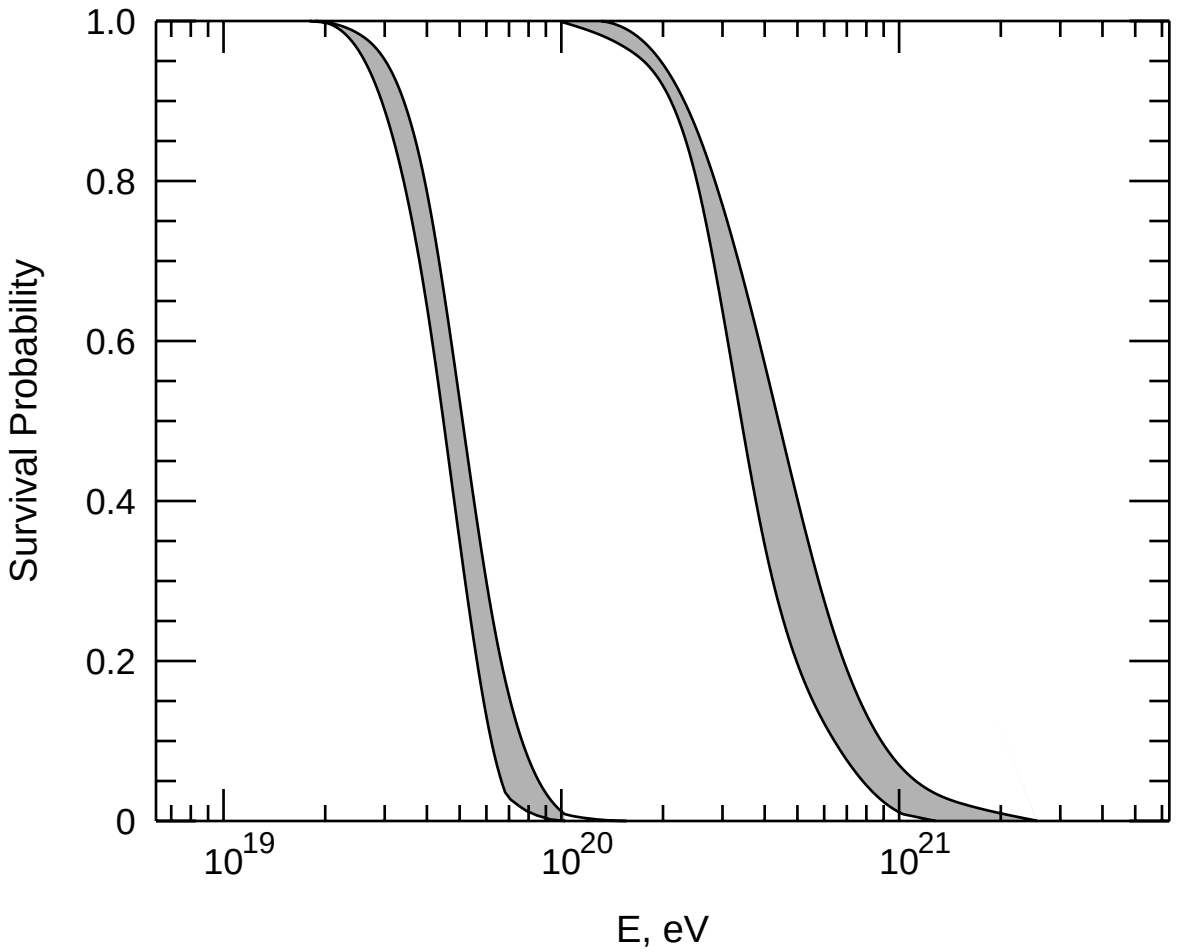

Stanev & Vankov, Fig. 4

Stanev & Vankov, Fig. 5

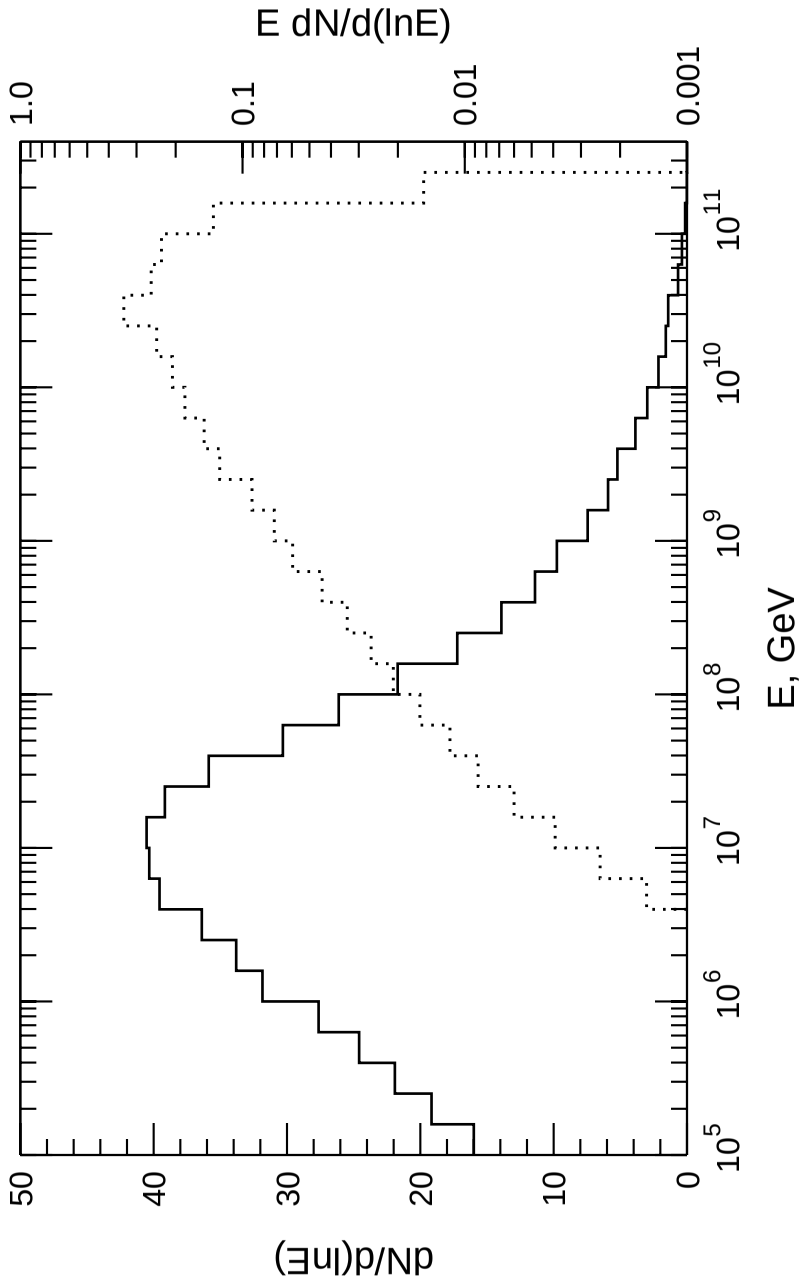

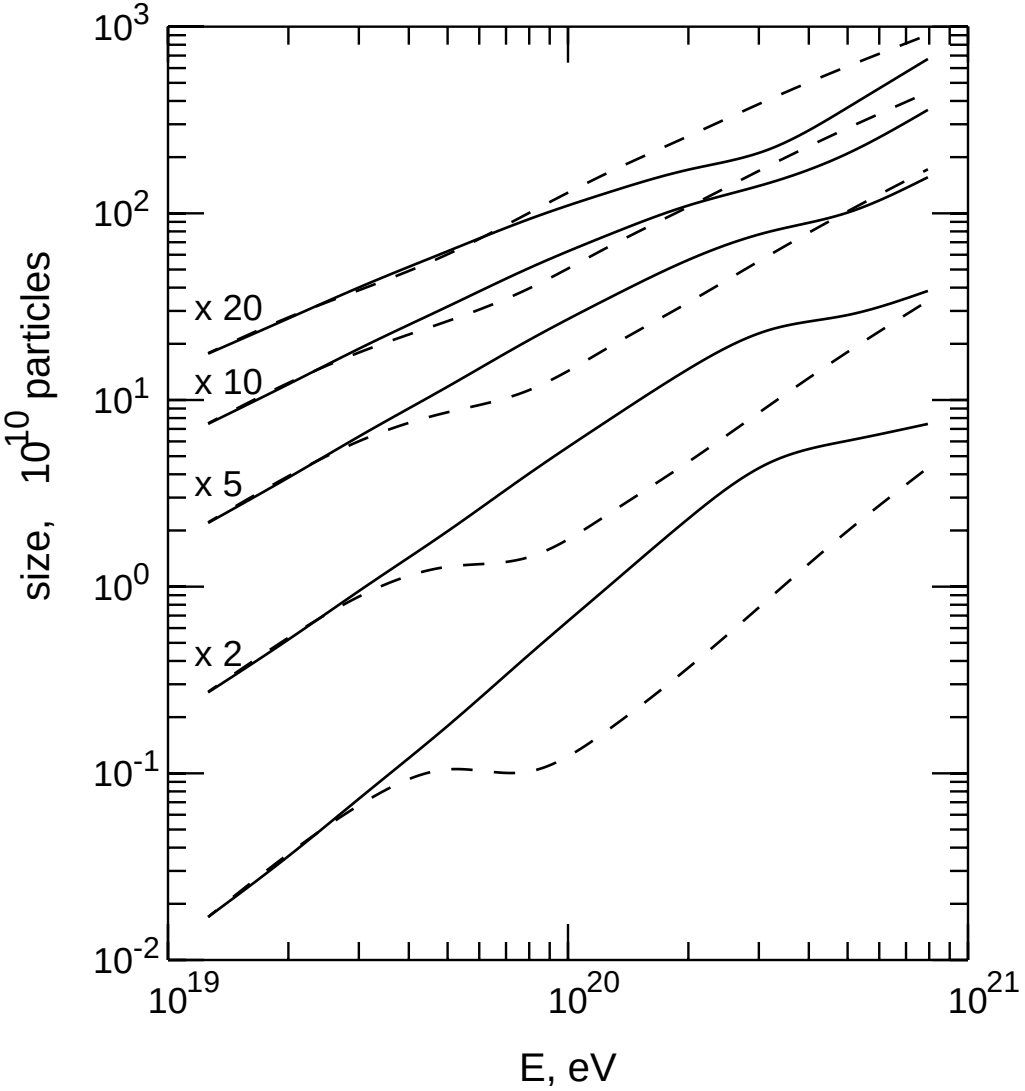

Stanev & Vankov, Fig. 6

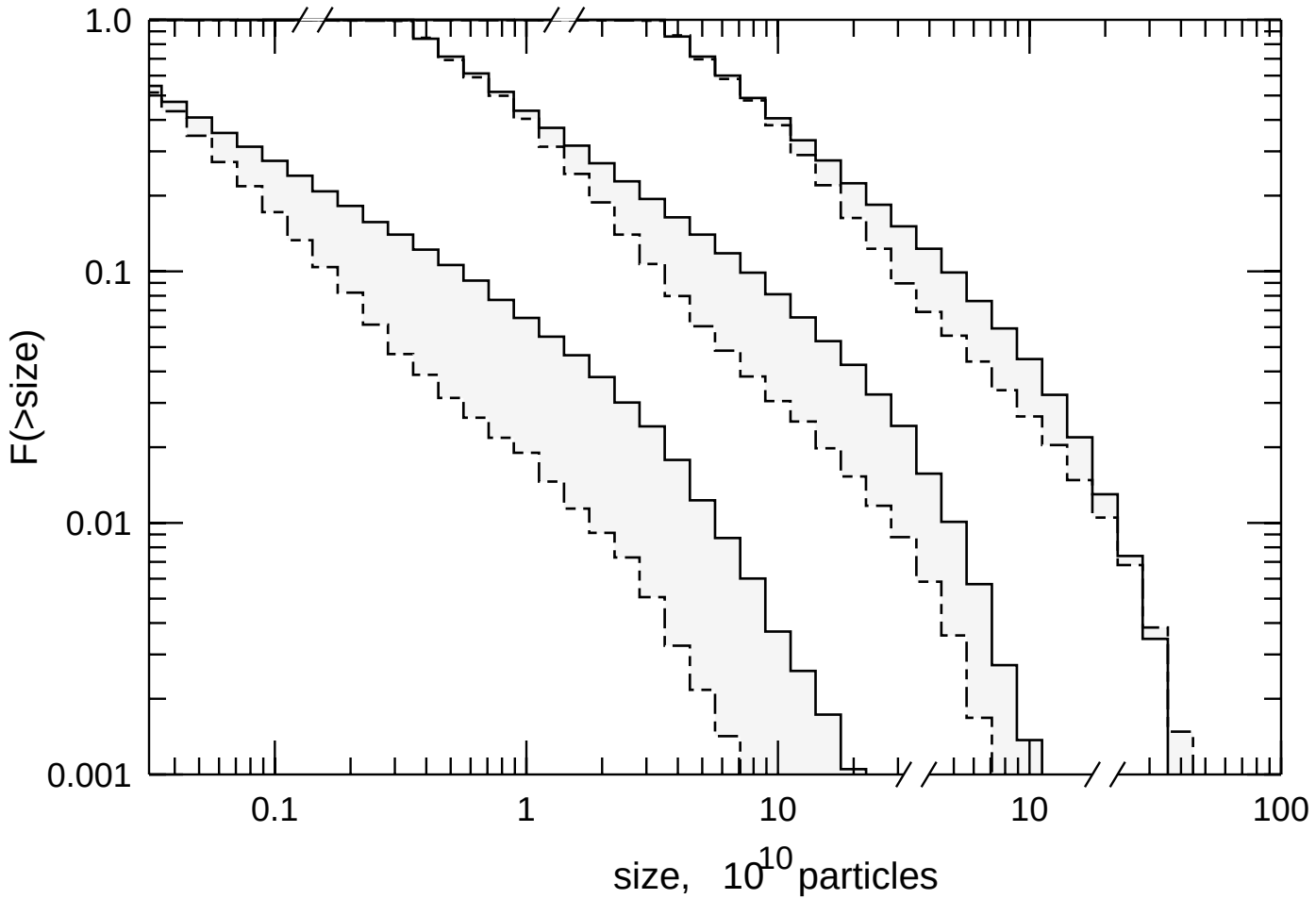

Stanev & Vankov, Fig. 7